

# Geology

## Warm and cold wet-states in the western United States during the Plio-Pleistocene --Manuscript Draft--

<b>Manuscript Number:</b>	G39962R1
<b>Full Title:</b>	Warm and cold wet-states in the western United States during the Plio-Pleistocene
<b>Short Title:</b>	Plio-Pleistocene wet-states in the western United States
<b>Article Type:</b>	Article
<b>Keywords:</b>	pluvial lakes, terrestrial hydroclimate, western North America, Budyko
<b>Corresponding Author:</b>	Daniel E Ibarra, B.S., M.S. Stanford University Stanford, California UNITED STATES
<b>Corresponding Author Secondary Information:</b>	
<b>Corresponding Author's Institution:</b>	Stanford University
<b>Corresponding Author's Secondary Institution:</b>	
<b>First Author:</b>	Daniel E Ibarra, B.S., M.S.
<b>First Author Secondary Information:</b>	
<b>Order of Authors:</b>	Daniel E Ibarra, B.S., M.S. Jessica L Oster, B.S., Ph.D. Matthew J Winnick, B.S., Ph.D. Jeremy K. Caves Rugenstein, B.S., Ph.D. Michael P Byrne, B.A., M.Sc., Ph.D. C. Page Chamberlain, B.S., M.S., Ph.D.
<b>Order of Authors Secondary Information:</b>	
<b>Manuscript Region of Origin:</b>	UNITED STATES
<b>Abstract:</b>	<p>The size distribution of lakes reflects the balance between the delivery of water through precipitation and its removal through evaporation. Lakes were abundant in the terminally draining basins of the western United States (U.S.) during both the colder-than-preindustrial latest Pleistocene glacial period (~14-29 ka) and the warmer-than-preindustrial mid-Pliocene (~2.9-3.3 Ma). To understand the hydroclimatic conditions that permitted lakes, we couple lake mass balance equations with a water and energy balance framework (sensu Budyko). Further, we compare paleo-lake area distributions to forward-modeled lake areas using climate model simulations of the Last Glacial Maximum (LGM, 19-26 ka) and mid-Pliocene. We conclude that both warmer- and colder-than-modern periods of the Plio-Pleistocene resulted in wetter-than-modern conditions in the terminally draining basins of the western U.S. through similar mechanisms. Specifically, the presence of lakes during the LGM reflects increased precipitation in addition to decreased temperatures, which decrease evaporative demand. In the southern Great Basin, LGM lakes require large increases in precipitation across the region. During the mid-Pliocene, increased evaporative demand necessitates increased precipitation to maintain lakes. Further, the increase in precipitation and dominantly southwestern distribution of mid-Pliocene lake deposits is consistent with proposed mean 'El-Niño-like' conditions altering regional hydroclimate during this period. These observations suggest that during interglacial periods the western U.S. resides within a local aridity maximum, and both long-term increases and decreases in global temperatures have been associated with wetter conditions across much of the western U.S. in the past.</p>

Publisher: GSA  
Journal: GEOL: Geology  
DOI:10.1130/G39962.1

1 Warm and cold wet states in the western United States  
2 during the Plio-Pleistocene

3 Daniel E. Ibarra<sup>1\*</sup>, Jessica L. Oster<sup>2</sup>, Matthew J. Winnick<sup>3</sup>, Jeremy K. Caves  
4 Rugenstein<sup>1,4</sup>, Michael P. Byrne<sup>5,6</sup>, and C. Page Chamberlain<sup>1</sup>

5 <sup>1</sup>*Earth System Science, Stanford University, Stanford, California 94305, USA*

6 <sup>2</sup>*Earth and Environmental Sciences, Vanderbilt University, Nashville, Tennessee 37240,*  
7 *USA*

8 <sup>3</sup>*Geological Sciences, Stanford University, Stanford, California 94305, USA*

9 <sup>4</sup>*Earth Sciences, ETH Zürich, 8092 Zürich, Switzerland*

10 <sup>5</sup>*Institute for Atmospheric and Climate Science, ETH Zürich, 8092 Zürich, Switzerland*

11 <sup>6</sup>*Space and Atmospheric Physics Group, Imperial College London, London SW7 2AZ, UK*

12 \*E-mail: danieli@stanford.edu

13 **ABSTRACT**

14 The size distribution of lakes reflects the balance between the delivery of water  
15 through precipitation and its removal through evaporation. Lakes were abundant in the  
16 terminally draining basins of the western United States (U.S.) during both the colder-  
17 than-preindustrial latest Pleistocene glacial period (~14–29 ka) and the warmer-than-  
18 preindustrial mid-Pliocene (~2.9–3.3 Ma). To understand the hydroclimatic conditions  
19 that permitted lakes, we couple lake mass balance equations with a water and energy  
20 balance framework (*sensu* Budyko). Further, we compare paleo-lake area distributions to  
21 forward-modeled lake areas using climate model simulations of the Last Glacial  
22 Maximum (LGM, 19–26 ka) and mid-Pliocene. We conclude that both warmer- and

colder-than-modern periods of the Plio-Pleistocene resulted in wetter-than-modern conditions in the terminally draining basins of the western U.S. through similar mechanisms. Specifically, the presence of lakes during the LGM reflects increased precipitation in addition to decreased temperatures, which decrease evaporative demand. In the southern Great Basin, LGM lakes require large increases in precipitation across the region. During the mid-Pliocene, increased evaporative demand necessitates increased precipitation to maintain lakes. Further, the increase in precipitation and dominantly southwestern distribution of mid-Pliocene lake deposits is consistent with proposed mean 'El-Niño-like' conditions altering regional hydroclimate during this period. These observations suggest that during interglacial periods the western U.S. resides within a local aridity maximum, and both long-term increases and decreases in global temperatures have been associated with wetter conditions across much of the western U.S. in the past.

## **INTRODUCTION**

The presence and size of lakes reflects the balance between moisture delivery and evaporative demand. Mid-latitude regions, such as the western United States (U.S.), exhibit evidence of large lake-level fluctuations during the Plio-Pleistocene in under-filled to balance-filled basins (Benson et al., 1990; Reheis et al., 2014; Pound et al., 2014). Barring large changes in rates of potential accommodation (i.e., tectonics), these fluctuations reflect changes in climate that control water and sediment supply to each basin's termini (cf. Carroll and Bohacs, 1999). Lacustrine deposits and paleo-shorelines found throughout the terminally draining (closed) basins of the western U.S. (Mifflin and Wheat, 1979; Reheis et al., 2014; Pound et al., 2014) suggest a hydrologic balance

dramatically different from the present during intervals of the Plio-Pleistocene (Matsubara and Howard, 2009; Ibarra et al., 2014; Oster et al., 2015; Barth et al., 2016; Putnam and Broecker, 2017).

We compile observations of lake presence and extent during the Last Glacial Maximum (LGM) and the mid-Pliocene. To understand what hydroclimatic factors permitted lake extents during these two periods, we use a framework that enforces mass and energy balance on precipitation-runoff relationships. We compare observations of the distributions of basin area-normalized lake areas to scaling of modern climatological distributions and climate model simulations.

## **METHODOLOGY**

### **Compilation of Geologic Observations**

We compile lake distributions for the LGM and mid-Pliocene in the western U.S. along with hydroclimate-sensitive proxies from previous studies (Dowsett et al., 1994; Molnar and Cane, 2007; Winnick et al., 2013; Oster et al., 2015) (Fig. 1). For the LGM, we use maps and tables of pluvial lake extent during the end of the last glacial cycle (~14–29 ka; Figure 1A; compiled in Table DR1<sup>1</sup>). Since terminally draining basin areas have not significantly shifted since the LGM (e.g., Benson et al., 1990; Reheis et al., 2014), we directly compare surface area estimates. Basin areas were derived from modern stream networks and watersheds from *HydroSHEDS* (<http://www.hydrosheds.org/>). We also account for recent work on the timing of pluvial lake highstands, which has demonstrated that lakes in the northern Great Basin (GB) reached maximum levels after the LGM, with LGM lake levels (stillstands) covering



~50–75% of the deglacial maximum areas (Benson et al., 1990; Ibarra et al., 2014; Reheis et al., 2014).

Pound et al. (2014) compiled the spatial distribution and estimated size of lakes during the mid-Pliocene warm period (defined as ~2.9–3.3 Ma for climate model simulations; Figure 1B) within the chronostratigraphically defined Late Pliocene (Piacenzian; 2.58–3.6 Ma), which we pair with modern drainage areas only in cases where the lake was terminal and drainage divides have not been greatly influenced by major tectonic drainage reconfiguration processes (DR text; Table DR3). Their lake size compilation is largely based on mapping and fish genetics work in southern California and southwestern Nevada, and other documented outcrops of Pliocene lacustrine sediments. Given that structural basin configurations are mostly unchanged since the Pliocene, it is possible that lakes filled the terminally draining basins in the GB during the Late Pliocene. As supporting evidence for lake presence, we also conducted a search for 2.9 to 3.3 Ma strata in *Macrostrat* (<https://macrostrat.org/>). We identified lacustrine strata that overlapped this range with sufficient thickness (>10 m of continuous sedimentation) to indicate a possible long-lived lake system (Fig. 1B). Tectonic and drainage capture processes may have influenced basin boundaries since the Pliocene, introducing potential uncertainties in quantitative comparisons; however, we note that the presence of lakes in terminally draining regions indicates a hydrologic balance wetter than modern.

### **Lake Areas and Hydroclimate Changes**

We combine a water and energy balance model with climate variables to forward-model lake areas. We extend a modeling framework proposed by Broecker (2010) by combining the commonly used basin area-normalized mass balance (cf. the pluvial

hydrologic index in Mifflin and Wheat, 1979) with a Budyko framework (cf. Broecker, 2010; Greve et al., 2015) to determine changes in precipitation-runoff scaling. For a terminally draining basin, the steady-state water balance is (Mifflin and Wheat, 1979; Broecker, 2010; Ibarra et al., 2014):

$$Pk_{\text{run}}(A_B - A_L) + PA_L = E_L A_L \quad (1),$$

where  $P$  is precipitation,  $k_{\text{run}}$  is a coefficient that determines the fraction of  $P$  converted to runoff,  $A$  is area (subscripts: terminal basin area ( $B$ ) and lake area ( $L$ )), and  $E_L$  is lake evaporation. Re-arranging, the proportional surface area of the lake relative to the basin area (Hudson and Quade, 2013) is:

$$\frac{A_L}{A_B} (\%) = \frac{Pk_{\text{run}}}{E_L - P + Pk_{\text{run}}} \times 100 \quad (2)$$

We relate lake evaporation ( $E_L$ ) to net radiation ( $R_N$ ) and temperature using the Priestley-Taylor equation (see DR text). To directly quantify the precipitation-runoff relationship under different climatic conditions, we impose a single-parameter Budyko curve constraint (cf. Broecker, 2010; Greve et al., 2015). We determine  $k_{\text{run}}$  as:

$$1 - k_{\text{run}} = \frac{ET}{P} = 1 + \frac{E_p}{P} - \left(1 + \left(\frac{E_p}{P}\right)^\omega\right)^{1/\omega} \quad (3),$$

where  $E_p$  is potential evapotranspiration,  $ET$  is evapotranspiration, and  $\omega$  is a free parameter that integrates the hydroclimatic properties of a watershed (Roderick et al., 2014; Greve et al., 2015). The Budyko framework ensures that lake water balance calculations are constrained to realistic bounds and imposes a nonlinear response of runoff to changes in precipitation. Previous work using more complex, hydrologic modeling for terminally draining basins in the GB (Matsubara and Howard, 2009; Barth et al., 2016) shows that for determining first-order trends in terminally draining basins

hydrologic simulations follow the precipitation-runoff relationship imposed by the  
Budyko framework.

We populate the parameters  $P$  and  $E_p$ , and assume  $\omega$  values (see below) in  
Equation 3 to solve for  $k_{run}$ , and  $P$ ,  $E_L$  and  $k_{run}$  in Equation 2 to solve for  $A_L/A_B$ . We use  
the energy, evapotranspiration, and precipitation fields from the North American  
Regional Reanalysis (NARR) for the modern sensitivity analysis, the Paleoclimate Model  
Intercomparison Project 3 (PMIP3; Braconnot et al., 2012) ensemble for the LGM (~21  
ka), and the Pliocene Model Intercomparison Project (PlioMIP; Haywood et al., 2013)  
ensemble for the mid-Pliocene (defined as 2.9-3.3 Ma). This analysis is implemented  
over model land grid-cells across the western U.S. (30–45 °N, 102–121 °W). For a subset  
of the analysis, we use a smaller region representing the southern GB (34–39 °N, 114–  
119 °W). Potential evapotranspiration ( $E_p$ ) is approximated as the liquid water equivalent  
of the net downward radiation at the surface ( $R_N$ ), which is balanced by the sensible ( $H$ )  
and latent ( $LE$ ) heat fluxes:

$$E_p = \frac{R_N}{L} = \frac{R_{S,i} - R_{S,o} + R_{L,i} - R_{L,o}}{L} = \frac{LE + H}{L} \quad (4),$$

where  $L$  is the latent heat of evaporation, and radiation ( $R$ ) subscripts denote  
incoming (i) and outgoing (o) long-wave (L) and short-wave (S) radiation (Roderick et  
al., 2014). These variables are taken as average annual sums from climate model  
simulations and NARR data for the domains in Figure 1.

We forward-model lake areas using climate model output to directly compare  
climate model simulations and observed lake area distributions. Using the climate model-  
derived  $E_p$  and  $P$  values, along with domain-wide  $\omega$  values derived from climate model's

individual output (see DR text), we calculate the runoff coefficient ( $k_{\text{run}}$ ) and derive normalized lake areas ( $A_L/A_B$ ).

To analyze the sensitivity of the regional water balance we use the distribution of the variables in Equations 2 and 4 from NARR (DR text). Using changes in temperature of  $-15$  to  $+10\text{K}$  relative to modern, we scale potential evapotranspiration ( $E_p = R_N/L$ ) by  $1.6\%/K$  and lake evaporation ( $E_L$ ) using the Priestley-Taylor equation (DR text). We scale precipitation from  $0.2x$  to  $3.25x$  of modern. For the sensitivity analysis,  $\omega = 2.6$  following Greve et al. (2015) (see DR text for further discussion). These ranges encapsulate proxy derived precipitation and temperature estimates for the mid-Pliocene and LGM intervals (Dowsett et al., 1994; Molnar and Cane, 2007; Matsubara and Howard, 2009). This normalization is consistent with other approaches that assess hydroclimate change relative to modern observations (e.g., Ibarra et al., 2014; Barth et al., 2016).

## PROXY COMPARISONS

The spatial distributions of lakes and moisture proxies during the LGM and mid-Pliocene (Fig. 1) were similar despite different background climate states. During the LGM, most terminally draining basins in the western U.S. contained lakes covering  $\sim 9.2\%$  ( $4.6\text{--}19.2\%$ , median and interquartile range (IQR)) of their basin areas, with the largest basin area-normalized lake areas located in the northern GB (up to  $49.0\%$ ). During the mid-Pliocene, early Piacenzian lake sediment areas compiled by Pound et al. (2014) are proportionally smaller and primarily located in the modern day southwest GB and Mojave Desert region (Fig. 1B). These lakes cover  $\sim 4.8\%$  ( $1.2\text{--}6.5\%$ ) of their basin areas, though we note large potential uncertainties in determining basin areas. Extant

(playa) lakes in the dry western GB (Table DR2) cover 1.0% (0.3–3.2%) of modern terminally draining basins.

*Macrostrat* suggests that Pliocene lakes existed elsewhere in the western U.S., likely within modern terminally draining basins (DR text). Proxy evidence from vegetation glaciers, speleothems and soils for the LGM suggests mostly drier than modern conditions approaching the ice sheet to the north, with some dry conditions east and northeast of the GB (Oster et al., 2015). Conversely, mid-Pliocene wet conditions appear to have extended farther east than the LGM (Fig. 1), consistent with proposed ‘El Niño-like’ climatological conditions involving a south-shifted Pacific storm track and increased precipitation (Molnar and Cane 2007; Winnick et al. 2013). Interpretation of wetter or drier conditions from vegetation records is complicated by the effect of changing atmospheric pCO<sub>2</sub> (Prentice et al., 2011; Scheff et al., 2017). Pollen records that indicate drier (wetter) conditions during the LGM (Pliocene) may in part be responding to lower (higher) atmospheric pCO<sub>2</sub> (~180 versus 400 ppm). Regardless, the distribution of wetter and drier pollen records supports the inferred spatial changes in hydroclimate from terminally-draining lakes in the LGM and mid-Pliocene.

## **HYDROLOGIC MODELING**

To better understand the role of temperature and precipitation in driving patterns of lake size distributions, we analyze how lake area cumulative distribution functions (CDFs) respond to changes in temperature (via  $E_L$ ,  $E_p$  and  $k_{run}$ ) and precipitation (Fig. 2A). We vary temperature and precipitation within the ranges described above assuming the modern median Budyko scaling parameter ( $\omega = 2.6$ ; Greve et al., 2015). Precipitation changes result in an increasing (decreasing) proportion of larger basin area-normalized

lake areas with increasing (decreasing) precipitation. Changes due to temperature are smaller in magnitude than those of precipitation with decreasing (increasing) temperatures causing increasing (decreasing) occurrence of large basin area-normalized lake areas.

In Figure 2C, we contour median (CDF = 0.5) normalized lake area to changes in precipitation and temperature. Assuming temperature estimates from other proxies for the western U.S. (Matsubara and Howard, 2009), we find that a majority of LGM lake levels are explained by moderate to large increases in precipitation (shaded blue IQR with precipitation factors of ~0.75–1.5 of modern (Matsubara and Howard, 2009; Ibarra et al., 2014)) accompanied by small decreases in evaporation. Further, decreased evaporative demand due to decreased temperature is of moderate importance for LGM lake areas when the distribution is adjusted to account for the observation that LGM stillstands were lower than the observed maximum highstands in the northern GB (Fig. DR3). In contrast, increased mid-Pliocene temperatures (Dowsett et al., 1994; Molnar and Cane, 2007) and the attendant increase in evaporative demand necessitate precipitation increases (Fig. 2C) to explain the distribution of lake areas, particularly when the southern GB is analyzed independently (shaded orange with IQR precipitation factor >1; Fig. 2D). Further, because the mid-Pliocene data have been derived primarily from basinal sedimentary deposits, which may have experienced subsequent erosion or burial, our distribution of mid-Pliocene areas may be an underestimate in precipitation increases.

Climate models and our proxy compilations demonstrate that LGM and mid-Pliocene precipitation and temperature changed in spatially heterogeneous ways, even in the sign of precipitation (cf. maps in Molnar and Cane, 2007; Oster et al., 2015). For

example, during the LGM, western U.S. precipitation exhibited a pronounced SW-NE dipole (Oster et al., 2015; Lora et al., 2017). When terminally draining basins in the southern portion of the GB are analyzed independently, they require large increases in precipitation (1.3x to 1.6x) to drive LGM lake levels because temperature decreased less than over inland terminally draining basins (Fig. 2D). Further, within the southern GB domain, the distribution of mid-Pliocene lakes (Fig. 1B) requires large precipitation increases (1.6x to 2.0x) to explain the presence of lakes (Fig. 2D).

Our sensitivity analyses does not account for spatially-variable anomalies. Therefore, we carry out similar calculations using climate model output (Fig. 2B). There is significant spread in the forward-modeled lake area anomalies. Notably, some LGM models have CDFs similar to the ensemble average CDF for the mid-Pliocene, and a comparison of these results to the distribution of lake areas (Table DR1) in Figure 2B shows agreement between the range of observations and the climate model output for both periods. However, because the region of interest is averaged over both terminally draining and open basins, and as the PMIP3/PlioMIP climate model simulations do not yet parameterize permanent lakes in their boundary conditions (cf. Pound et al., 2014), the climate model distributions in Figure 2B show more heavily-tailed distributions than the range of observations, which suggest maximum basin area-normalized lake areas of 49% for LGM and 13% for the mid-Pliocene.

## IMPLICATIONS

Hydroclimate in the western U.S. responded nonlinearly to past climatic forcings. Increased precipitation with reduced evaporative demand resulted in wetter conditions during colder-than-preindustrial periods. Further, increased moisture convergence may

have been a mechanism for wetter conditions during warmer-than-preindustrial periods. Consequently, the interglacial western U.S. appears to represent a local aridity maximum that is transitional between two different wet states, resulting in the fewest and smallest lakes compared to geologically-recent colder and warmer periods. Thus, past climatic change did not result in unidirectional changes in the regional water balance; rather, the interplay between thermodynamic and dynamic effects results in a more complex, nonlinear response. The mechanism of increased moisture convergence during the mid-Pliocene is beyond the scope of this study. However, the existence of background “El Niño-like” conditions, driven by reduced meridional and zonal sea surface temperature gradients (Burls and Fedorov, 2017), may have strengthened southwesterly moisture delivery (Molnar and Cane 2007; Winnick et al., 2013; Haywood et al., 2013), resulting in greater wintertime precipitation that fed lakes in the southwest U.S. While the direct applicability of mid-Pliocene conditions to future warming scenarios remains unclear (Burls and Fedorov, 2017), our results suggest that if future warming results in similar “El Niño-like” tropical Pacific conditions, aridity may decrease in the western U.S.

Our analysis demonstrates how differences in regional atmospheric moisture divergence and convergence along with regional water/energy balances (e.g., Seager et al. 2014; Putnam and Broecker, 2017) are recorded in lacustrine sediments and shoreline deposits. Future work to better constrain lake and terminally-draining basin areas for under-constrained geologic time slices, such as the mid-Pliocene, will provide new constraints on the terrestrial hydroclimate response to climatic change.

## ACKNOWLEDGMENTS



249 We thank Alan Carroll and three anonymous reviewers for thorough reviews. We  
250 thank P.J. Dennedy-Frank, K. Maher, T.J. Kukla, and A.J. Ritch. We acknowledge the  
251 climate modeling groups for making output available, and PCMDI and A. Haywood for  
252 output distribution. This work was supported by NSF EAR-1450357 to Chamberlain.

253 **REFERENCES CITED**

- 254 Barth, C., Boyle, D.P., Hatchett, B.J., Bassett, S.D., Garner, C.B., and Adams, K.D.,  
255 2016, Late Pleistocene climate inferences from a water balance model of Jakes  
256 Valley, Nevada (USA): *Journal of Paleolimnology*, v. 56, p. 109–122,  
257 <https://doi.org/10.1007/s10933-016-9897-z>.
- 258 Benson, L.V., Currey, D.R., Dorn, R.I., Lajoie, K.R., Oviatt, C.G., Robinson, S.W.,  
259 Smith, G.I., and Stine, S., 1990, Chronology of expansion and contraction of four  
260 great Basin lake systems during the past 35,000 years: *Palaeogeography*,  
261 *Palaeoclimatology, Palaeoecology*, v. 78, p. 241–286, [https://doi.org/10.1016/0031-](https://doi.org/10.1016/0031-0182(90)90217-U)  
262 [0182\(90\)90217-U](https://doi.org/10.1016/0031-0182(90)90217-U).
- 263 Braconnot, P., Harrison, S.P., Kageyama, M., Bartlein, P.J., Masson-Delmotte, V., Abe-  
264 Ouchi, A., Otto-Bliesner, B., and Zhao, Y., 2012, Evaluation of climate models using  
265 palaeoclimatic data: *Nature Climate Change*, v. 2, p. 417–424,  
266 <https://doi.org/10.1038/nclimate1456>.
- 267 Broecker, W., 2010, Long-term water prospects in the Western United States: *Journal of*  
268 *Climate*, v. 23, p. 6669–6683, <https://doi.org/10.1175/2010JCLI3780.1>.
- 269 Burls, N.J., and Fedorov, A.V., 2017, Wetter subtropics in a warmer world: Contrasting  
270 past and future hydrological cycles: *Proceedings of the National Academy of*

- 271 Sciences of the United States of America, v. 114, p. 12888–12893,  
272 <https://doi.org/10.1073/pnas.1703421114>.
- 273 Carroll, A.R., and Bohacs, K.M., 1999, Stratigraphic classification of ancient lakes:  
274 Balancing tectonic and climatic controls: *Geology*, v. 27, p. 99–102,  
275 [https://doi.org/10.1130/0091-7613\(1999\)027<0099:SCOALB>2.3.CO;2](https://doi.org/10.1130/0091-7613(1999)027<0099:SCOALB>2.3.CO;2).
- 276 Dowsett, H., Thompson, R., Barron, J., Cronin, T., Fleming, F., Ishman, S., Poore, R.,  
277 Willard, D., and Holtz, T., Jr., 1994, Joint investigations of the Middle Pliocene  
278 climate I: PRISM paleoenvironmental reconstructions: *Global and Planetary Change*,  
279 v. 9, p. 169–195, [https://doi.org/10.1016/0921-8181\(94\)90015-9](https://doi.org/10.1016/0921-8181(94)90015-9).
- 280 Greve, P., Gudmundsson, L., Orlowsky, B., and Seneviratne, S.I., 2015, Introducing a  
281 probabilistic Budyko framework: *Geophysical Research Letters*, v. 42, p. 2261–  
282 2269, <https://doi.org/10.1002/2015GL063449>.
- 283 Haywood, A.M., et al., 2013, Large-scale features of Pliocene climate: results from the  
284 Pliocene Model Intercomparison Project: *Climate of the Past*, v. 9, p. 191–209,  
285 <https://doi.org/10.5194/cp-9-191-2013>.
- 286 Hudson, A.M., and Quade, J., 2013, Long-term east-west asymmetry in monsoon rainfall  
287 on the Tibetan Plateau: *Geology*, v. 41, p. 351–354,  
288 <https://doi.org/10.1130/G33837.1>.
- 289 Ibarra, D.E., Egger, A.E., Weaver, K.L., Harris, C.R., and Maher, K., 2014, Rise and fall  
290 of late Pleistocene pluvial lakes in response to reduced evaporation and precipitation:  
291 Evidence from Lake Surprise, California: *Geological Society of America Bulletin*,  
292 v. 126, p. 1387–1415, <https://doi.org/10.1130/B31014.1>.

- 293 Lora, J.M., Mitchell, J.L., Risi, C., and Tripathi, A.E., 2017, North Pacific atmospheric  
294 rivers and their influence on western North America at the Last Glacial Maximum:  
295 Geophysical Research Letters, v. 44, p. 1051–1059,  
296 <https://doi.org/10.1002/2016GL071541>.
- 297 Matsubara, Y., and Howard, A.D., 2009, A spatially explicit model of runoff,  
298 evaporation, and lake extent: Application to modern and late Pleistocene lakes in the  
299 Great Basin region, western United States: Water Resources Research, v. 45,  
300 p. W06425, <https://doi.org/10.1029/2007WR005953>.
- 301 Mifflin, M.D., and Wheat, M.M., 1979, Pluvial lakes and estimated pluvial climates of  
302 Nevada: Nevada Bureau of Mines and Geology Bulletin, v. 95, 57 p.
- 303 Molnar, P., and Cane, M.A., 2007, Early Pliocene (pre–Ice Age) El Niño–like global  
304 climate: Which El Niño?: Geosphere, v. 3, p. 337–365,  
305 <https://doi.org/10.1130/GES00103.1>.
- 306 Oster, J.L., Ibarra, D.E., Winnick, M.J., and Maher, K., 2015, Steering of westerly storms  
307 over western North America at the Last Glacial Maximum: Nature Geoscience, v. 8,  
308 p. 201–205, <https://doi.org/10.1038/ngeo2365>.
- 309 Pound, M.J., Tindall, J., Pickering, S.J., Haywood, A.M., Dowsett, H.J., and Salzmann,  
310 U., 2014, Late Pliocene lakes and soils: a global data set for the analysis of climate  
311 feedbacks in a warmer world: Climate of the Past, v. 10, p. 167–180,  
312 <https://doi.org/10.5194/cp-10-167-2014>.
- 313 Prentice, I.C., Harrison, S.P., and Bartlein, P.J., 2011, Global vegetation and terrestrial  
314 carbon cycle changes after the last ice age: The New Phytologist, v. 189, p. 988–998,  
315 <https://doi.org/10.1111/j.1469-8137.2010.03620.x>.

- Putnam, A.E., and Broecker, W.S., 2017, Human-induced changes in the distribution of rainfall: *Science Advances*, v. 3, p. e1600871, <https://doi.org/10.1126/sciadv.1600871>.
- Reheis, M.C., Adams, K.D., Oviatt, C.G., and Bacon, S.N., 2014, Pluvial lakes in the Great Basin of the western United States-a view from the outcrop: *Quaternary Science Reviews*, v. 97, p. 33–57, <https://doi.org/10.1016/j.quascirev.2014.04.012>.
- Roderick, M.L., Sun, F., Lim, W.H., and Farquhar, G.D., 2014, A general framework for understanding the response of the water cycle to global warming over land and ocean: *Hydrology and Earth System Sciences*, v. 18, p. 1575–1589, <https://doi.org/10.5194/hess-18-1575-2014>.
- Scheff, J., Seager, R., Liu, H.B., and Coats, S., 2017, Are Glacials Dry? Consequences for Paleoclimatology and for Greenhouse Warming: *Journal of Climate*, v. 30, p. 6593–6609, <https://doi.org/10.1175/JCLI-D-16-0854.1>.
- Seager, R., Neelin, D., Simpson, I., Liu, H., Henderson, N., Shaw, T., Kushnir, Y., Ting, M., and Cook, B., 2014, Dynamical and Thermodynamical Causes of Large-Scale Changes in the Hydrological Cycle over North America in Response to Global Warming\*: *Journal of Climate*, v. 27, p. 7921–7948, <https://doi.org/10.1175/JCLI-D-14-00153.1>.
- Winnick, M.J., Welker, J.M., and Chamberlain, C.P., 2013, Stable isotopic evidence of El Niño-like atmospheric circulation in the Pliocene western United States: *Climate of the Past*, v. 9, p. 903–912, <https://doi.org/10.5194/cp-9-903-2013>.

**FIGURE CAPTIONS**

339

340 Figure 1. Maps of lakes and hydroclimate-sensitive proxies. A: LGM lake extents are  
341 compiled in Table DR1. B: Mid-Pliocene lake locations are included from Pound et al.  
342 (2014) and from *Macrostrat*. The mid-Pliocene and LGM proxy networks are coded as  
343 indicating wetter, drier, or no change relative to modern. Dashed boxes denote the  
344 analysis domains.

345

346 Figure 2. Climatic forcing and lake area changes. A: Scaling of modern climate  
347 distributions (CDFs) to linear changes in precipitation and temperature. Bold line is  
348 modern. B: Basin area-normalized lake area using climate model simulations relative to  
349 modern for the western U.S. domain. C: Median basin area-normalized lake area (CDF =  
350 0.5 from panel A) contoured for changes in precipitation and temperature for the same  
351 domain. Shaded regions are the IQR with thick median lines of the observed lake areas  
352 and the range of temperature change estimates relative to modern. D: Same as C for the  
353 southern GB domain.

354

355 1GSA Data Repository item 2018xxx, dataset compilation and modeling description, is  
356 available online at <http://www.geosociety.org/datarepository/2018/> or on request from  
357 [editing@geosociety.org](mailto:editing@geosociety.org).

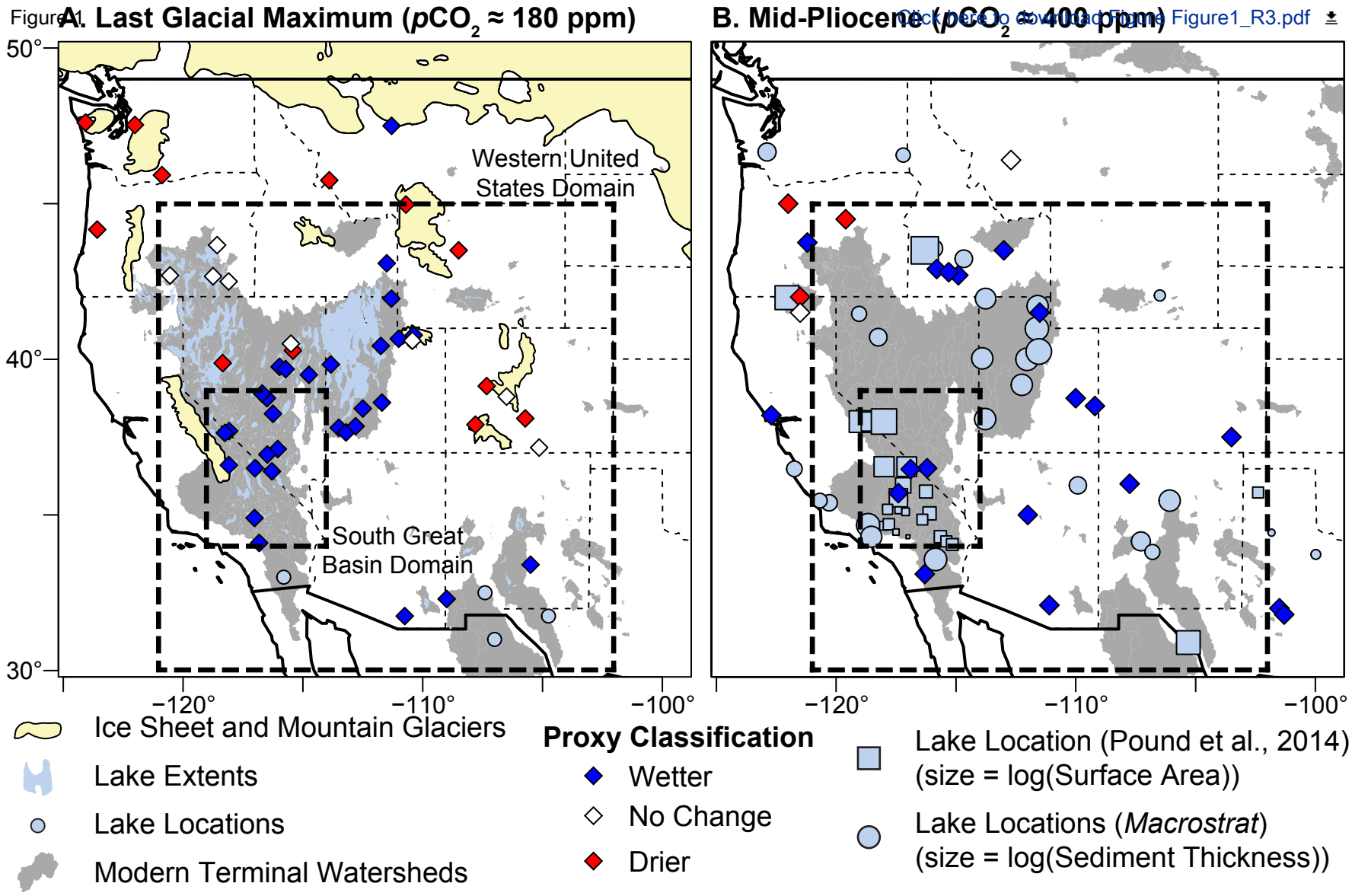
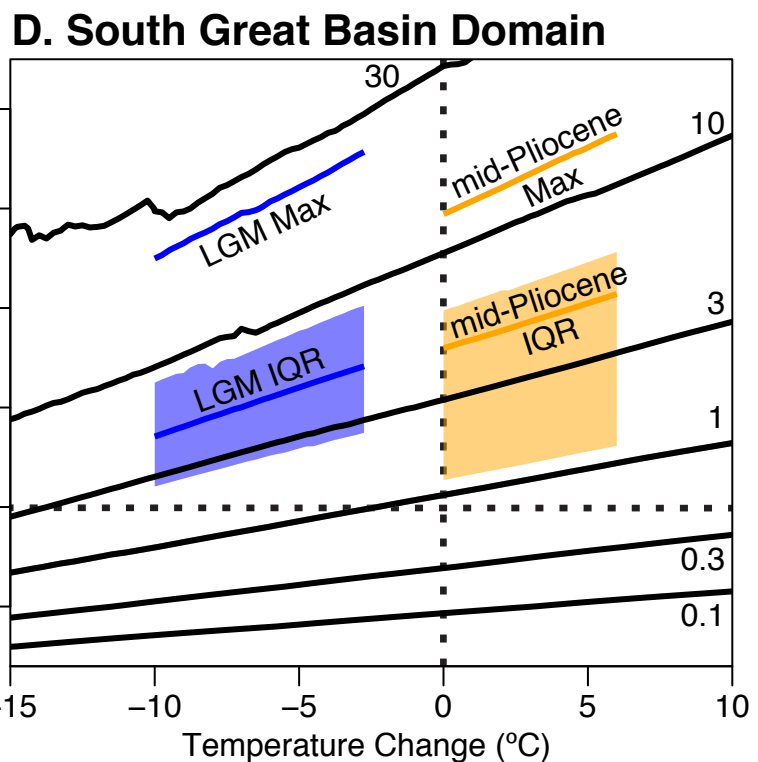
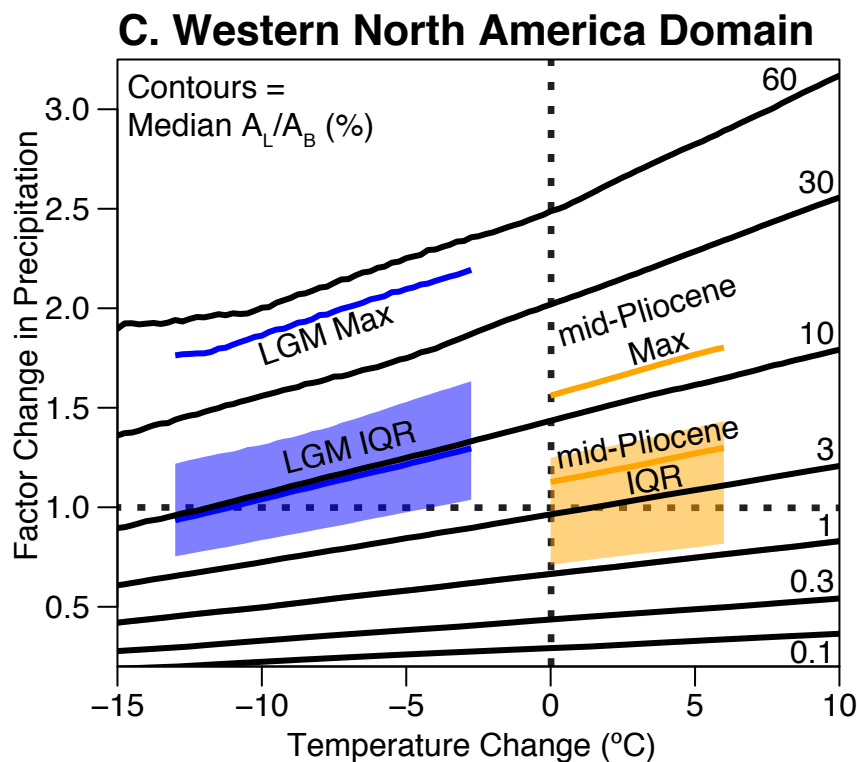
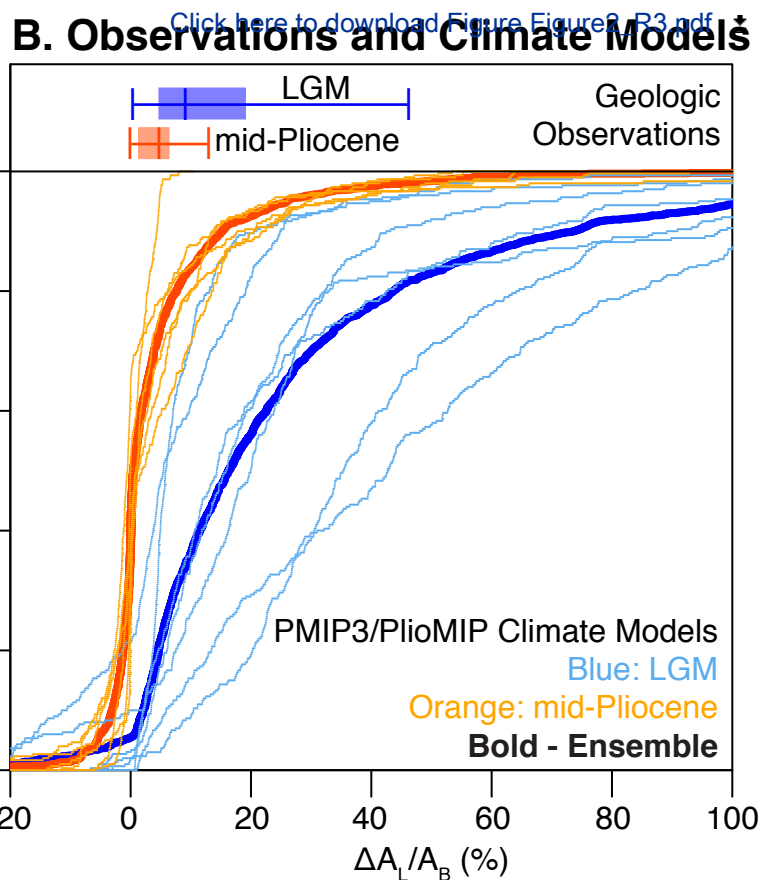
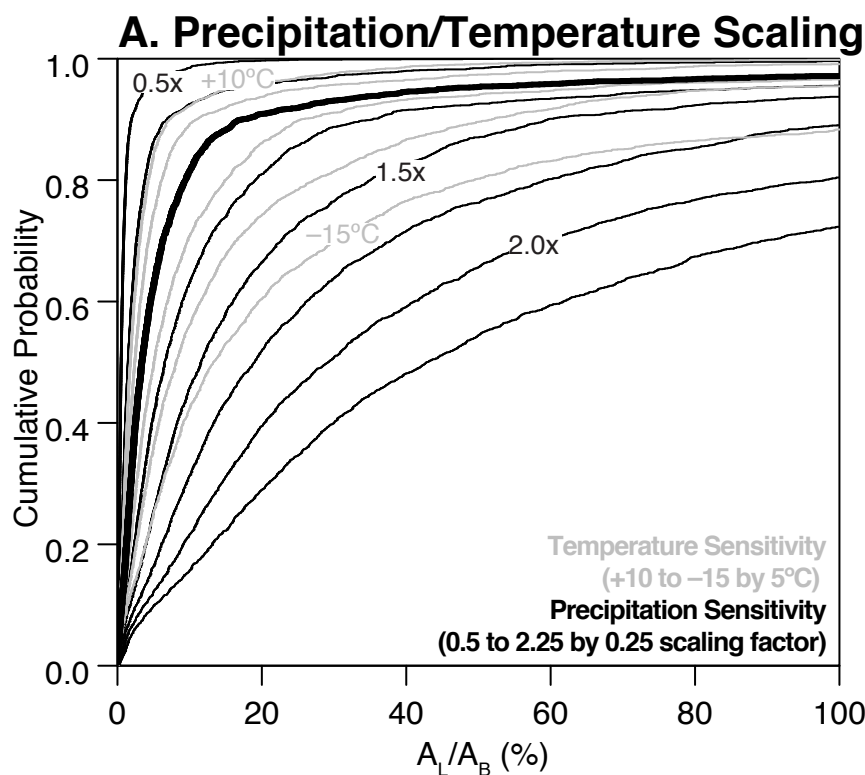


Figure 2



**GSA Data Repository 2018xxx**

## **Warm and cold wet-states in the western United States during the Plio-Pleistocene**

Daniel E. Ibarra<sup>1\*</sup>, Jessica L. Oster<sup>2</sup>, Matthew J. Winnick<sup>3</sup>,  
Jeremy K. Caves Rugenstein<sup>1,4</sup>, Michael P. Byrne<sup>5,6</sup>, and C. Page Chamberlain<sup>1</sup>

<sup>1</sup>*Earth System Science, Stanford University, Stanford, California 94305, USA*

<sup>2</sup>*Earth and Environmental Sciences, Vanderbilt University, Nashville, Tennessee 37240, USA*

<sup>3</sup>*Geological Sciences, Stanford University, Stanford, California 94305, USA*

<sup>4</sup>*Earth Sciences, ETH Zürich, 8092 Zürich, Switzerland*

<sup>5</sup>*Institute for Atmospheric and Climate Science, ETH Zürich, 8092 Zürich, Switzerland*

<sup>6</sup>*Space and Atmospheric Physics Group, Imperial College London, London SW7 2AZ, UK*

Date Repository Contents:

- Scaling of potential evapotranspiration with surface temperature
- Processing of climate model output and NARR dataset
- Dataset Treatment
- Figures DR1-DR3
- Links to databases used for this study
- Tables DR1-DR5
- DR References



### Scaling of potential evapotranspiration with surface temperature

We use climate model experiments to estimate how net surface radiation ( $R_N$ ) and potential evapotranspiration ( $E_p$ ) scale with temperature (Equation 4). To do so we sum the radiation fluxes (Equation 4) to obtain the annual net surface radiation ( $R_N$ ) and calculate average annual temperature for all land grid cells in our domain of interest (30-45 °N, 102-121 °W). We then calculate domain average temperature and  $R_N$  anomalies for the LGM and Pliocene using the PMIP3 and PlioMIP output (Table DR5) relative to the preindustrial control experiments (see next section). We also include 25 CMIP5 climate models using 30-year averages from the historical (1976-2005) and RCP 8.5 (2070-2099) simulations (where the historical period is taken as the control point). The  $R_N$  anomalies are calculated as a percentage change relative to the control.

The potential evapotranspiration calculated from the net surface radiation scales with surface temperature at a rate of 1.6%/K (Figure DR1). For this study we use the net-radiation formulation of potential evapotranspiration (Roderick et al., 2014) and thus use the scaling factor of 1.6%/K for the NARR sensitivity analyses. This regional result derived using the CMIP5, PMIP3 and PlioMIP models is similar to previous work using CMIP3 and CMIP5 models which suggest empirical scalings of  $R_N$  to temperature of ~0.9 to 1.5 %/K (Milly and Dunne, 2016; Scheff and Frierson, 2014; Roderick et al., 2014; 2015).

### Processing of climate model output and NARR dataset

To carry out our lake area modeling (Equations 2 and 3), we use monthly average output from the North American Regional Reanalysis (NARR) (Mesinger et al., 2006), the Paleoclimate Model Intercomparison Project 3 (PMIP3) ensemble and the Pliocene Model Intercomparison Project (PlioMIP) ensemble (Braconnot et al., 2012; Haywood et al., 2011; 2013). PlioMIP conducted two distinct simulations; we choose to use Experiment 2, which is the full ocean-atmosphere climate model simulations of the mid-Pliocene (*cf.* Haywood et al., 2013), making them more directly comparable to the LGM model output from PMIP3. We only use the archived energy and precipitation fields for forward modeling lake area distributions (Equation 2), and follow Roderick et al. (2014) by also using evapotranspiration (ET) fields to derive estimates of the regional  $\omega$  parameters used in the Budyko equation (Equation 3). The models used in this study (Table DR4) are a subset of the PMIP3 and PlioMIP ensembles that included all of the necessary surface energy and water flux variables necessary to carry out our calculations. Because of different model resolutions we re-grid all model data prior to further analysis using the ‘fields’ package in R (Nycha et al. 2016).

We use the methods outlined by Roderick et al. (2014) and process the NARR and climate model output by calculating the annual sum of potential evapotranspiration ( $E_p$ ) as the liquid water equivalent of the net irradiance (Equation 4 in main text). Further, annually summed precipitation (P) and evapotranspiration were tabulated from monthly averages. We use all of the land-grid cells where ET does not exceed P annually to fit the Budyko relationship (Equation 3 in main text) using the ‘nls2’ package in R (Grothendieck, 2013). The derived  $\omega$  values are reported in Table DR5. The median change in  $E_p/P$  vs.  $ET/P$  for all grid cells in the domain for each model is shown in Figure DR2 with the mean  $\omega$  value over all models contoured. We plot the median change of  $E_p/P$  vs.  $ET/P$ , rather than mean changes, for each individual model because the spatial distributions of  $E_p$ , P and ET are skewed in the modeling domain of interest. To avoid potential biases in absolute precipitation amount simulated by different models, we plot the anomaly relative to the pre-industrial control simulation in the predicted lake surface area

change in Figure 2B rather than the absolute value. Further, since our objective is to model trends and lake area distributions, we determine  $E_L$  using the Priestley-Taylor equation (Priestley, 1959; Priestley and Taylor, 1972; Sumner and Jacobs, 2005):

$$LE = \alpha \frac{\Delta}{\Delta + \gamma} R_N \quad (\text{DR1})$$

where  $LE$  is the latent heat flux that is related to lake evaporation ( $E_L$  in equation 3 in the main text) by the latent heat of vaporization,  $\alpha=1.25$  is an empirically determined dimensionless correction,  $\Delta$  is the slope of the saturation vapor-pressure curve, which is temperature dependent,  $\gamma$  is the psychrometric constant, which is elevation dependent, and  $R_N$  is the net downward radiation at the surface (see equation 4). Use of more complex evaporation equations would require additional parameters that are difficult to estimate or measure in the past (e.g., Linacre, 1977).

To carry out the NARR sensitivity analyses (Figure 2A, 2C, 2D and DR3), we scale precipitation linearly using a scaling factor as described in the main text. Temperature is scaled linearly to scale  $R_N$  (equation 4) by 1.6%/K (see previous section). Further, because we use the Priestley-Taylor equation (Priestley, 1959; Priestley and Taylor, 1972; Sumner and Jacobs, 2005) to approximate lake evaporation ( $E_L$  in equation 2 in the main text) changes in temperature change the slope ( $\Delta$ ) of the saturation vapor-pressure curve. For the NARR sensitivity analyses, we use the US catchment median value of  $\omega = 2.6$  (Greve et al., 2015). If we were to use a lower  $\omega$  value (see for example PMIP3/PliomIP control simulations in Table DR5), as suggested by maps of modern catchment derived  $\omega$  values in Greve et al. (2015), the effect of decreasing evaporative demand on increasing LGM lake levels would be greater, suggesting lower precipitation scaling factors (Figure 2C and 2D). Conversely, the increase in precipitation needed to drive Pliocene lake areas would be lower, but greater than pre-industrial. However, a majority of the models suggest a decrease in  $\omega$  for the LGM but not the Pliocene (Table DR5).

## Dataset Treatment

**LGM Normalized Lake Areas.** LGM lake areas were compiled from the tables and maps of the sources listed in Table DR1 (Allen, 2005; Reheis, 1999; Orme, 2008; Grayson, 2011; *Natural Earth* database; Soller et al., 2009; Williams and Bedinger, 1984; Mifflin and Wheat, 1979). We assume no major watershed boundary and basin configuration changes since the LGM. We paired the lake areas in ArcGIS 10.0 with the LGM lake areas with modern watershed boundaries from the *HydroSHEDS*, *HydroBASINS*, and *HydroLAKES* (Lehner et al., 2008; Lehner and Grill, 2013; Messenger et al., 2016) databases (<http://www.hydrosheds.org/>). Further assumptions were:

- Average normalized areas were calculated across all available estimates (rightmost column of Table DR1).
- For Figure DR3 northern Great Basin lakes ( $> 39^\circ\text{N}$ ) areas were reduced by 50%, based on work from smaller lakes such as Lake Surprise (Ibarra et al., 2014), Lake Franklin (Munroe and Laabs, 2013), and a review by Reheis et al. (2014).

**Mid-Pliocene Normalized Lake Areas.** Lake areas were only derived from the compilation in Pound et al. (2014). We only paired lakes in the compilation from Pound et al. (2014) to modern drainage basins (Table DR3) if the following criteria were met:

- It was clear that the lake was terminal based on the lacustrine sedimentology, topography and drainage network (cf. Table 2 in Pound et al. (2014)).
- The lake area did not span multiple modern watersheds over large drainage divides nor did it appear to be influenced by large tectonic drainage reconfigurations (cf. Adam et al., 1990; Thompson, 1992; Reheis et al., 2002; Knott et al., 2008; Phillips, 2008; Pound et al., 2014).

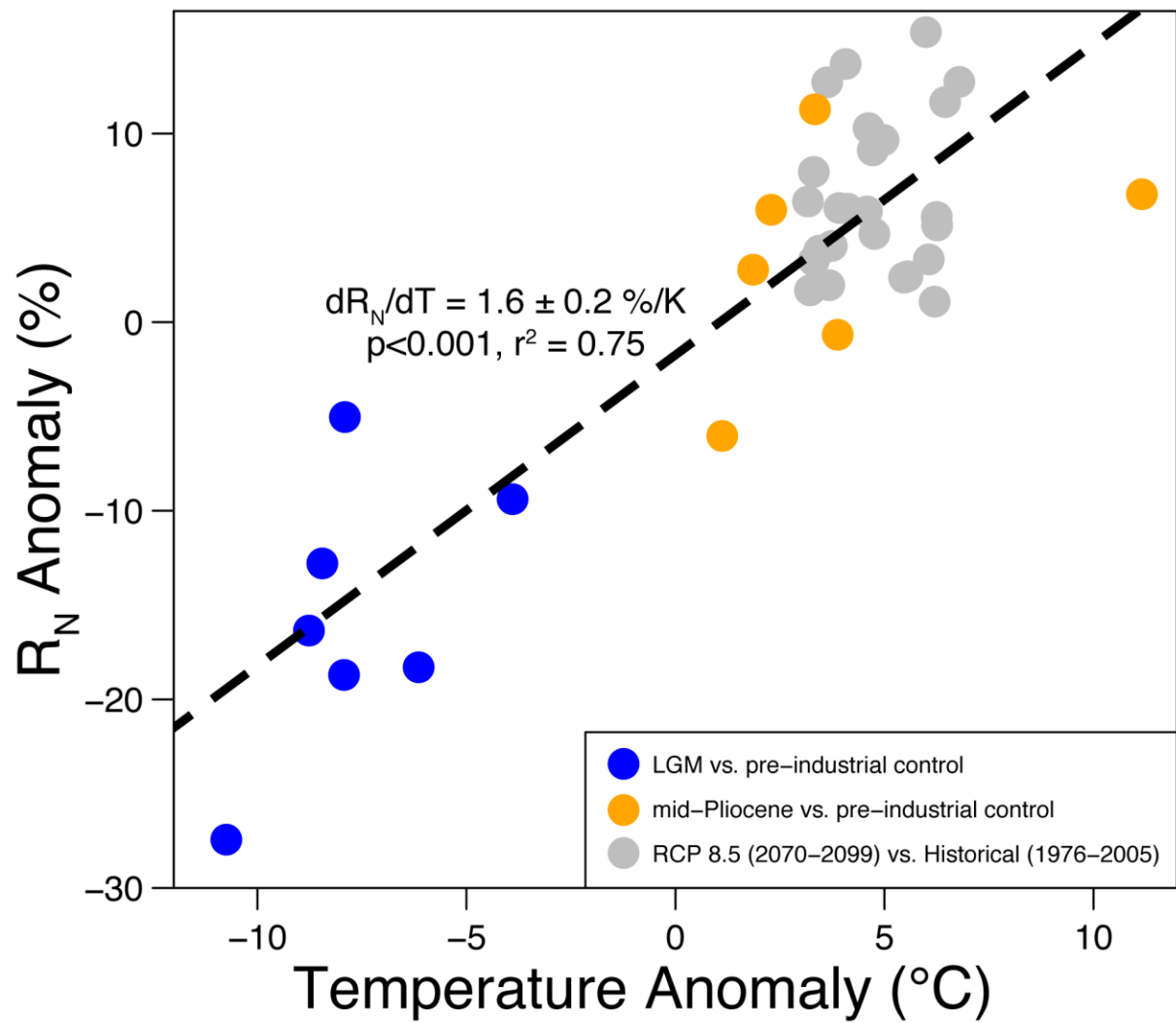
Given that extension in the Basin and Range has been ongoing since the Miocene (e.g., Colgan et al., 2006), it is likely that the many terminal basins created by Basin and Range faulting were filled by lakes during wet intervals such as the mid-Pliocene. Since the Pound et al. (2014) dataset is primarily derived from basinal sedimentary deposits, which may have undergone unquantifiable erosion or burial since Pliocene deposition the  $A_L/A_B$  calculations may be underestimates which would necessitate even larger increases in precipitation relative to present day during the mid-Pliocene. However, if additional extension has occurred since the Pliocene these estimates may be overestimates. Examples of lakes in Table DR 3 from the Pound et al. (2014) compilation for which normalized lake areas were not calculated include Tule Lake (Adam et al., 1990), which has evidence for a sill indicating that the lake overflowed into the Klamath River basin (cf. Figure 1 of Adam et al., (1990)), and Glenn's Ferry (Smith, 1981; Thompson, 1992), due to possible drainage to the southwest (Thompson, 1992).

*Macrostrat* lacustrine data are only used as supporting evidence plotted on Figure 1B. The *Macrostrat* database does not provide individual lakes, rather the database contains aggregates of stratigraphic datasets grouped into polygons of differing areas. However, given the relatively high resolution of the *Macrostrat* polygons the distribution of mid-Pliocene lacustrine sediments suggests that many areas of modern terminally draining basins had lakes during the mid-Pliocene (Fig. 1B).

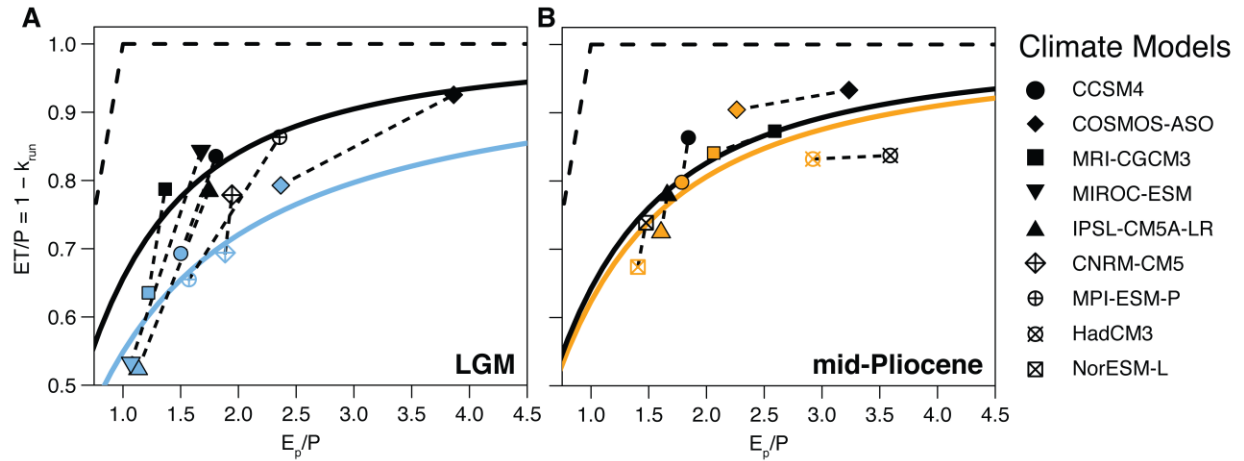
The calculation of lake area,  $A_L$  represents the maximum expansion of lakes in a given basin during the time intervals of interest. A complication for both the LGM and mid-Pliocene lake areas is the "Manly Group", which contain multiple higher elevation fill and spill sub-basins that eventually flowed to Lake Manly (Death Valley). For ease of analysis we choose to group these sub-basins into one large terminal basin (see Table DR1 and DR3) although this treatment may result in an underestimate in  $A_L/A_B$ . Similarly, Lake Lahontan and Lake Bonneville integrated multiple sub-basins but were fully connected at their highstand elevations (Reheis et al., 2014). As such, we combined areas for all sub-basins in the Lahontan and Bonneville watersheds in Table DR1.

**Temperature Estimates.** Independent estimates of temperature changes (relative to modern) (x-axis of Figures 2C, 2D and DR3) are as follows:

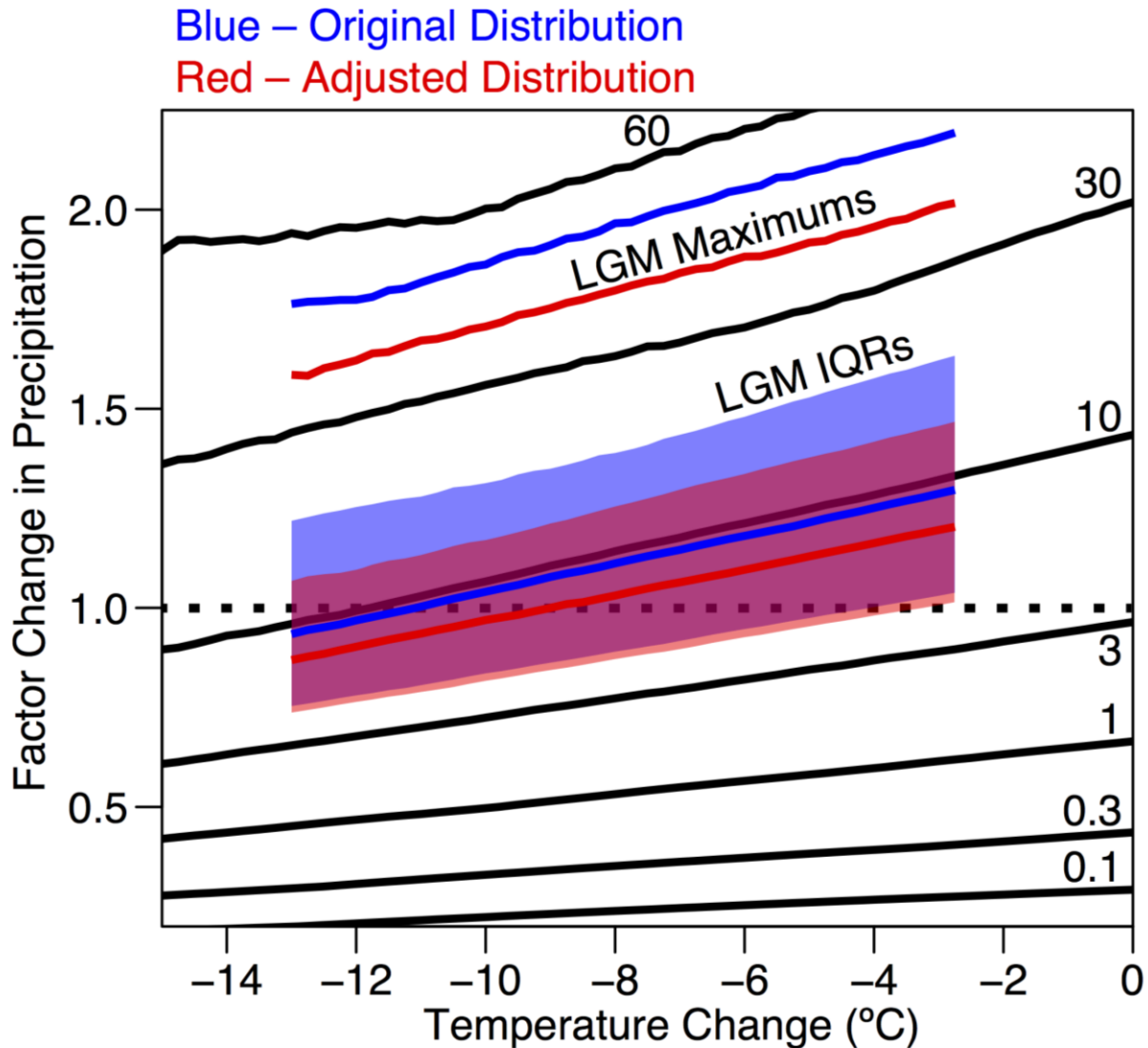
- Figure 2C we plot the full range of temperature estimates for the LGM (-13 to -2.75 °C (median = -7.5°C) based on tables in: Matsubara and Howard, 2008; Grayson, 2011).
- In Figure 2D depressions are observed to be less depressed in this region than further inland. Thus, we plot a reduced range of temperature estimates for the LGM (-10 to -2.75 °C based on tables in: Matsubara and Howard, 2008; Grayson, 2011).
- For Figures 2C and 2D we plot the full range of temperature estimates for the mid-Pliocene (0 to +6 °C based on tables in: Dowsett et al., 1994; Molnar and Cane, 2007)



**DR1.** Empirical scaling of potential evapotranspiration with surface temperature based on PMIP3, PlioMIP and CMIP5 simulations (see DR text above).



**DR2. A:** Budyko framework – median changes in  $E_p/P$  vs.  $ET/P$  calculated from LGM climate model simulations. Dashed lines connect simulations from the same models. Colored curves and symbols are the LGM simulations. Solid lines are the ensemble averages (Table DR5). See climate model processing methods for more details. **B:** Same as A for mid-Pliocene simulations.



**DR3.** Effect of adjusting northern Great Basin lake areas. Median calculated lake level from NARR data (black lines) and original LGM distributions (blue shading and lines) are the same as Figure 2C. Shown in red is the adjusted distribution of LGM lake areas (see Table DR1) assuming ~50% smaller lakes in the northern Great Basin (lakes north of 39 °N). Many lakes in the northern Great Basin stood at prominent but lower stillstands during the LGM than the post-LGM highstands (Munroe and Laabs, 2013; Ibarra et al., 2014; Reheis et al., 2014). As in Figure 2B we plot the full range of temperature estimates for the LGM (-13 to -2.75 °C (median = -7.5°C) based on tables in: Matsubara and Howard, 2008; Grayson, 2011).

### **Links to online databases for geospatial and climate data used for this study**

- *HydroSHEDS/HydroBASINS/HydroLAKES* (Lehner et al., 2008; Lehner and Grill, 2013; Messenger et al., 2016): <http://www.hydrosheds.org/>
- *Natural Earth* pluvial lakes database: <http://www.naturalearthdata.com/downloads/10m-physical-vectors/10m-lakes/>
- *Macrostrat* database: <https://macrostrat.org/>
- “Extent of Pleistocene Lakes in the Western Great Basin”, by Reheis (1999): <https://geonsdi.er.usgs.gov/metadata/map-mf/2323/metadata.faq.html>
- “Map Database for Surficial Materials in the Conterminous United States”, by Soller et al. (2009): <https://pubs.usgs.gov/ds/425/>
- NCEP North American Regional Reanalysis (NARR): <https://www.esrl.noaa.gov/psd/data/gridded/data.narr.html>
- Paleoclimate Modelling Intercomparison Project 3 (PMIP3): <https://pmip3.lscce.ipsl.fr/>
- PlioMIP1 output was distributed by Alan Haywood, Aislin Dolan, Daniel Hill and Steven Pickering (personal communication, 2016)

**Table DR1 – Compilation of late Pleistocene (~LGM) lake areas and modern watershed areas.** All areas are in km<sup>2</sup>. References: (1) *HydroSHEDS/HydroBASINS/HydroLAKES* (Lehner et al., 2008; Lehner and Grill, 2013; Messenger et al., 2016), (2) Allen (2005), (3) Reheis (1999), (4) Orme (2008), (5) Grayson (2011), (6) *Natural Earth* database, (7) Soller et al. (2009), (8) Williams and Bedinger (1984), (9) Mifflin and Wheat (1979). Average normalized areas are calculated using the *HydroBASINS* (Lehner and Grill, 2013) basin areas and stream networks with all available lake area estimates (columns 2b, 3a, 4-9). Agreement of lake areas between publications is <5% for most basins. Allen (2005) basin areas (column 2a) are for comparison only. Reheis (1999) maximum lake areas (column 3b) are not used as they represent post-LGM highstand areas or pre-MIS 2 highstands. Latitude and longitude values are for reference only and correspond to the centroid for each terminal basin. Soller et al. (2009), Reheis (1999) and the *Natural Earth* pluvial lakes database are mapped in Figure 1A. Adjusted normalized distributions (shown used in Figure DR3) assumes that LGM lake areas were ~50% maximum highstands for watersheds north of 39 °N (polygon centroid's location) to account for post-LGM highstands observed in the northern Great Basin (Munroe and Laabs, 2013; Ibarra et al., 2014; Reheis et al., 2014). Unnamed basins were assigned numbers: UN-GB# – Unnamed-Great Basin; UN-SW# – Unnamed-Southwest.

Lake Name	Latitude	Longitude	Basin Area (1)	Basin Area (2a)	Lake Area (2b)	Lake Area (3a)	Maximum Lake Area (3b)	Lake Area (4)	Lake Area (5)	Lake Area (6)	Lake Area (7)	Lake Area (8)	Lake Area (9)	Average Normalized Area (%)
Acme	38.55	-118.32	351.45							7.40				2.10
Alford	42.18	-118.68	7031.36			1153.62		1270.00	1269.10	947.19		1217.30		16.66
Alkali	43.04	-120.06	1375.20					550.00	590.52	565.90				41.36
Animas	32.29	-108.85	5607.00	5670.00	374.00						313.38			5.59
Antelope	39.85	-114.31	874.68			140.15			124.32	127.12		124.32	124.32	14.64
Bonneville	40.18	-112.67	134131.13					51700.00	51864.55	51956.71		51644.40	51644.40	38.59
Bonnie Claire	37.33	-117.11	3526.21							142.63				4.04
Bristol	37.96	-114.76	2334.47						90.65	77.33		90.65		3.69
Buffalo	40.50	-117.32	1284.38			66.55			199.43	195.25		199.43		12.86
Cactus Flat	38.13	-116.80	6100.73					344.47		374.97				5.90
Cahuilla	33.00	-115.80	20050.8									7769.97		38.75
Carpenter	38.51	-114.57	1432.29			121.93			347.06	358.10		347.06	347.06	21.24
Catlow	42.52	-119.20	4850.63					900.00	898.73	905.54		1152.55		19.88
Cave	38.57	-114.85	930.13			121.29			178.71	180.27		178.71	178.71	18.01
Cedar	37.62	-113.17	374.57							18.55				4.95
Chewaucan	42.68	-120.51	3385.35					1200.00	1243.20	1194.08		1243.20		36.04
Chochise	32.15	-109.84	4357.00								545.79	621.60		13.40
Clayton	37.71	-117.60	1437.76							85.14				5.92
Clover	40.85	-114.83	2665.56			743.21	1094.25	890.00	890.96	913.81		911.68	911.68	32.90
Cloverdale	31.36	-108.85	467.80	460.00	102.00						82.52	77.70		17.12
Coal	38.00	-115.41	2487.57						178.71	188.33		178.71	178.71	7.28
Colombus	37.79	-118.00	3532.12			141.45			139.86	365.10		204.61	204.61	5.98
Coyote	42.38	-118.19	1789.45			317.39				125.90				12.39
Cuddeback	35.31	-117.47	555.31									90.65		16.32
Deep Spring	37.36	-118.08	519.42						44.03	25.33		44.03		7.28
Delamar	37.44	-114.87	926.74							26.49				2.86
Desatoya	39.29	-117.57	1490.65			397.51			435.12	442.13		435.12	435.12	28.78
Diamond	39.40	-116.38	8018.15			1021.21	2283.22	760.00	758.87	1023.04		1015.28		11.42
Dixie	39.80	-117.84	5410.24			798.63	2394.69	1090.00	1090.39	721.47		714.84	766.64	15.96
Eagle	40.64	-120.89	1123.78			126.84			160.58	145.49				12.84
Edwards	39.58	-117.69	1078.89			287.10			264.18	266.36		264.18	264.18	24.95
Encino	34.60	-105.60	644.20	620.00	96.00						56.77	310.80		28.53
Estancia	34.67	-105.96	5733.70	5050.00	1125.00						1084.76	2330.99		29.79
Fort Rock	43.28	-120.89	6403.89						1945.08	1564.66		2343.94		30.47



Franklin	40.37	-115.23	3345.89			947.49		1220.00	1219.89	1248.19		1250.97	1250.97	35.55
Fred	39.77	-119.82	47.73							7.90				16.56
Frenchman	36.85	-115.96	1180.75							20.05				1.70
Gabbs	38.85	-118.09	3319.81							312.43				9.41
Gale	39.83	-115.09	1912.71			168.82			411.81	431.64		411.81		18.61
Garfield	38.36	-118.32	246.58						7.77	17.47		7.77	8.55	4.21
Gilbert	39.84	-116.71	1540.94			392.61		540.00	538.72	398.62		401.45		29.48
Gold Flat	37.50	-116.50	1791.85						67.34	66.76		67.34	67.34	3.75
Goldfield	37.85	-117.29	826.72							17.75				2.15
Goodsight	32.50	-107.33	532.20	590.00	65.00							38.85		7.30
Granite Springs	40.25	-118.89	2518.64						103.60	109.41		103.60	103.60	4.17
Groom	37.31	-115.86	1717.34						93.24	74.32		93.24		5.06
Groom	37.23	-115.41	2575.13							133.60		93.24		4.40
Guano	42.00	-119.48	2124.41							172.02				8.10
Harper	35.06	-117.33	1871.58									139.86		7.47
High Rock	42.02	-119.16	194.06							13.95		31.08		11.60
Hubbs	39.76	-115.37	1666.22			532.16	619.98	530.00	530.95	521.93		505.05	505.05	31.26
Huntoon	38.11	-118.58	318.05							5.39				1.69
Indian Springs	36.68	-115.73	1719.03							168.33				9.79
Jakes	39.30	-115.27	1102.26			213.14			163.17	155.12		163.17	163.17	15.56
Kawich	37.49	-116.22	947.41						56.98	49.12		56.98	56.98	5.81
Kumiva	40.43	-119.12	853.07						38.85	45.10		38.85	38.85	4.74
Labou	39.23	-118.27	790.86			35.64			51.80	50.69		51.80	51.80	6.11
Lahontan	40.36	-118.09	105613.36			21906.48	30917.97	22300.00	22004.56	23368.63		21859.52	23478.78	21.29
Laughton	39.68	-119.97	81.36						18.13	10.87		18.13		19.31
Lemmon	39.67	-119.87	247.58						33.67	37.94		33.67	33.67	14.03
Little Fish	38.84	-116.42	1055.41							12.67				1.20
Lunar Crater	38.66	-115.98	1291.56							16.17				1.25
Luning	38.46	-118.10	637.12							30.56				4.80
Macy	41.97	-119.66	76.41							20.35		23.31		28.57
Madeline	40.89	-120.38	2167.64					780.00	777.00	763.23		777.00		35.72
Malheur	43.44	-119.11	13083.89					2380.00	2380.20	2432.95		2460.49		18.45
Manly Group	36.20	-117.16	51541.38						4169.88	5004.85				8.90
Maxey	38.76	-114.42	1370.13			210.87			209.79	211.83		209.79	209.79	15.36
Meinzer	41.59	-119.73	1870.75			923.61		920.00	919.45	992.93		890.96	890.96	49.34
Monte Cristo	38.34	-117.80	720.59							14.26				1.98
Mormon	36.84	-115.40	973.54							70.35				7.23
Newark	39.38	-115.82	3604.16			816.84	986.44	930.00	795.13	805.90		782.18	782.18	22.72
Otero	32.86	-106.36	9556.70	12600.00	745.00						409.94	466.20		4.58
Pahrump	36.05	-115.81	3748.99							657.73				17.54
Papoose	37.08	-115.81	256.83							27.20				10.59
Penoyer	37.74	-115.79	1819.15							59.39				3.26
Pine	38.45	-113.74	1898.09				922.41		106.19	116.43				5.86
Pinos Wells	34.46	-105.60	589.90	560.00	82.00						49.11	207.20		21.72
Playas	31.86	-108.57	1135.60	1120.00	49.00						16.72	259.00		12.14
Railroad	38.65	-115.67	5518.75			864.43		1360.00	1359.74	980.86		971.25	971.25	19.65
Reveille	38.22	-116.22	4346.40			146.20			106.19	103.75		106.19	106.19	2.62
Rhodes	38.25	-118.11	520.42						33.67	29.66		33.67	33.67	6.28
Sacramento	32.46	-105.66	1397.40	780.00	86.00									6.15
Saline	36.78	-117.78	1928.51							83.93				4.35
San Agustin	33.85	-108.15	3046.90	3880.00	786.00						513.47	1129.24		26.96

Snyder	38.84	-116.07	163.65							38.98				23.82
Spring	39.45	-114.47	2949.98			617.85		870.00	870.24	640.32		603.47	603.47	23.76
Stonewall	37.63	-116.94	938.60							49.80				5.31
Surprise	41.35	-119.98	3840.91			1477.95		1310.00	1310.53	1475.66		1471.11	1484.84	37.01
Teel	38.13	-118.37	810.54							42.30				5.22
Thompson	34.92	-118.02	9115.90					950.00	950.53			556.85		8.99
Toiyabe	39.10	-117.02	3411.50			421.96		650.00	650.09	573.98		525.77	525.77	16.35
Tonopah	38.42	-117.51	5294.27			277.56			233.10	264.91		233.10	233.10	4.69
Trinity	33.55	-106.56	4524.50	4240.00	207.00						134.57	199.43		3.69
UN-GB1	35.76	-116.83	43.73							3.73				8.53
UN -GB2	35.70	-116.77	360.86							2.72				0.75
UN -GB3	37.14	-117.22	249.07							4.34				1.74
UN-GB4	37.17	-117.83	1540.52							6.55				0.43
UN-GB5	36.76	-117.53	162.92							6.25				3.84
UN-GB6	35.55	-116.69	402.92							4.78				1.19
UN-GB7	35.44	-113.80	3674.90								300.82			8.19
UN-SW1	34.14	-107.61	882.90								49.73			5.63
UN-SW10	33.47	-102.49	936.20								20.46			2.19
UN-SW11	33.76	-102.52	702.40								54.71			7.79
UN-SW12	33.98	-102.55	200.50								19.16			9.56
UN-SW13	33.89	-102.98	1653.40								51.41			3.11
UN-SW14	33.68	-103.68	82.80								15.54			18.77
UN-SW15	34.85	-103.99	49.30								14.32			29.05
UN-SW2	31.77	-102.88	2437.20								19.49			0.80
UN-SW3	31.50	-102.67	340.80								15.02			4.41
UN-SW4	31.47	-102.52	696.00								17.44			2.51
UN-SW5	31.68	-101.88	202.60								14.15			6.99
UN-SW6	32.39	-102.66	103.70								32.83			31.66
UN-SW7	32.91	-102.29	421.70								35.39			8.39
UN-SW8	33.13	223.12	222.00								47.14			21.23
UN-SW9	33.44	-102.07	688.90								19.94			2.89
Waring	40.00	-114.65	8566.76			1375.87		2520.00	1331.25	1686.23		1401.18	1401.18	18.90
Warner	42.40	-119.90	4804.82			1331.27		1250.00	1250.97	1202.50		1307.94		26.40
Yahoo	39.47	-116.09	44.62						5.18	6.97		5.18	5.18	12.61
Yucca	37.09	-116.08	777.53							12.39				1.59
													Normalized Area (%) Distribution	
													Median	9.20
													Q1	4.62
													Q3	19.17
													Max	49.34
													Adjusted Normalized Area (%) Distribution	
													Median	7.30
													Q1	4.32
													Q3	13.62
													Max	38.75
													South Great Basin (%) Distribution	
													Median	5.06
													Q1	2.62
													Q3	8.53
													Max	23.82

**Table DR2 –Area of modern lakes (>1km<sup>2</sup>) found in terminal watersheds.** Data derived from the HydroSHEDS/HydroLAKES/HydroBASINS database (Lehner et al., 2008; Lehner and Grill, 2013; Messenger et al., 2016) intended to represent maximum possible sizes by including seasonal playa lakes.

Lake Name	Basin Area	Total Lake Area	Normalized Area (%)	Notes
Alkali	1375.20	14.97	1.09	3 unnamed seasonal playa lakes
Alvord	7031.36	5.49	0.08	Seasonal playa lake
Bonneville	134131.13	8923.51	6.65	Maximum size: Great Salt Lake, Bonneville Salt Flats, Bear Lake and other playa lakes
Chewaucan	3385.35	285.86	8.44	Lake Abert and Summer Lake
Clover	2665.56	5.13	0.19	Playa Lake
Fort Rock	6403.89	8.24	0.13	Seasonal playa Lake
Franklin	3345.89	13.17	0.39	3 playa/marsh lakes
Lahontan	105613.36	954.70	0.90	Pyramid and Walker Lakes (historic areas) plus playa lakes
Malheur	13083.89	422.28	3.23	2 playa lakes
Manly Group	51541.38	238.52	0.46	Includes area of Mono Lake (Pleistocene Lake Russell) and seasonal playa lakes in all following sub-basins: Owens, Searles, Panamint, Manly
Meinzer	1870.75	56.33	3.01	Numerous small seasonal playa lakes
Spring	2949.98	4.07	0.14	Playa lake
Surprise	3840.91	255.13	6.64	3 seasonal playa lakes
Warner	4804.82	130.15	2.71	Numerous small seasonal playa lakes
		<b>Area Normalized (%) Distribution</b>		
		<b>Median</b>	1.00	
		<b>IQR1</b>	0.24	
		<b>IQR3</b>	3.17	
		<b>Max</b>	8.44	

**Table DR3 – Compilation of mid-Pliocene (early Piacenzian, ~2.9 to 3.3 Ma) lake deposits.** P2014 – Pound et al. (2014). We consider all continuous formations that span the Piacenzian in *Macrostrat*. Pliocene lake areas are only paired to basin areas when it is clear that the lake was terminal, does not span multiple modern watersheds over large drainage divides, and have not been greatly influenced by tectonic drainage reconfiguration.

Name of Lake/Formation	Latitude	Longitude	Reference	Age minimum (Ma)	Age maximum (ma)	Thickness (m)	Unit ID	Section ID	
Palouse Loess	46.56	-117.2	Macrostrat	0	3.3	100	7460	1968	
	36.42	-115.43	Macrostrat	0	5.3	10	14059	3727	
	38.08	-113.78	Macrostrat	0	17.1	1000	14212	3774	
Santa Fe Gp	35.46	-106.08	Macrostrat	0	14.4	1000	14906	3965	
Paso Robles Fm	35.39	-120.29	Macrostrat	0	5.3	200	17724	4603	
Santa Fe Gp	34.15	-107.28	Macrostrat	0.7	4.9	470	2187	356	
Santa Fe Gp	33.81	-106.8	Macrostrat	0.7	4.9	130	2214	362	
Glenns Ferry Fm	43.56	-115.92	Macrostrat	0.7	5.8	300	7488	1975	
	40.71	-118.24	Macrostrat	0.7	4.9	300	13530	3584	
Atherton Fm	38.63	-87.07	Macrostrat	1.5	5.1	50	11687	3158	
Fort Hancock Fm	31.91	-106.5	Macrostrat	1.9	3.6	10	1889	292	
Santa Fe Gp	33.05	-105.61	Macrostrat	1.9	19.3	10	2275	383	
Paso Robles Fm	35.46	-120.68	Macrostrat	1.9	8.3	120	17735	4605	
Paso Robles Fm	36.48	-121.74	Macrostrat	1.9	8.3	155	17753	4612	
Blanco Fm	33.73	-99.98	Macrostrat	2.6	3.3	24	2575	469	
Hungry Valley Fm	34.67	-118.66	Macrostrat	2.6	4.9	2000	6314	1522	
Palm Spring Fm	33.57	-115.85	Macrostrat	2.6	3.3	1500	6544	1598	
Salt Lake Fm	41.95	-113.76	Macrostrat	2.6	8.7	800	14128	3752	
	40.03	-113.9	Macrostrat	2.6	17.1	1000	14210	3773	
Salt Lake Fm	41.71	-111.59	Macrostrat	2.6	17.1	1000	14476	3839	
Salt Lake Fm	40	-112.03	Macrostrat	2.6	10.5	1500	14565	3863	
	40.55	-112.3	Macrostrat	2.6	17.1	10	14626	3885	
Salt Lake Fm	40.98	-111.62	Macrostrat	2.6	19.3	2000	14722	3909	
Salt Lake Fm	40.25	-111.54	Macrostrat	2.6	17.1	4000	14727	3910	
Bidahochi Fm	35.95	-109.91	Macrostrat	2.6	5.3	272	14987	3988	
Bug Fm	42.05	-106.49	Macrostrat	2.6	4	37	15759	4174	
Tule Gp	34.43	-101.83	Macrostrat	2.8	2.9	10	2528	458	
Gila Conglomerate	32.48	-108.26	Macrostrat	2.8	4	10	1855	271	
Sunshine Ranch Mbr of Saugus Fm	34.3	-118.53	Macrostrat	2.8	3.1	915	6344	1529	
	46.66	-122.88	Macrostrat	2.8	13.3	350	7257	1896	
Glenns Ferry Gp	43.23	-114.67	Macrostrat	2.8	8.3	300	13673	3622	
	39.18	-112.25	Macrostrat	2.8	12.2	1000	14570	3864	
Thousand Creek Beds	41.46	-119.04	Macrostrat	2.9	8.3	130	13454	3543	
						Outcrop or Lake Area (km²)	Normalized Area (%)	Age minimum (Ma)	Age maximum (ma)
Glenn's Ferry, ID	43.50	-116.30	P2014		Not terminal	22144		2.4	3.8
Tule Lake	41.98	-122.05	P2014		Not terminal?	6291.45		2.6	3
Rhodes-Clayton-Fish Valleys, NV	38.00	-118.00	P2014		Watershed unclear	10800		2.6	3.4
Owens Lake	36.55	-118.00	P2014		Larger Manly Basin	1500		2	3
Lake Manly	36.55	-117.05	P2014		Larger Manly Basin	1300		2	3
Panamint Lake	35.95	-117.20	P2014		Larger Manly Basin	276		2	3
China-Scarles Lake	35.55	-117.40	P2014		Larger Manly Basin	800		2	3
Kochn Lake_1	35.18	-117.85	P2014		Larger Manly Basin	40		2	3

Kochn Lake_2	35.15	-117.40	P2014		Larger Manly Basin	12.5		2	3
Kochn Lake_3	35.10	-117.10	P2014		Larger Manly Basin	16		2	3
Lake Russell	38.00	-119.00	P2014		Mono and Lake Russell listed separately by P2014	2800		2	2.8
Mono Lake	38.00	-118.55	P2014		Mono and Lake Russell listed separately by P2014	1125		2	3
All Manly Basin with Lake Russell Area			P2014	51541		6744.5	13.09		
Harper_1	34.65	-118.00	P2014		Watershed unclear	25		2	3
Harper_2	34.65	-117.90	P2014		Watershed unclear	4		2	3
Harper_3	34.70	-117.80	P2014	750	Assumed separate from Harper 4	60	8.00	2	3
Harper_4	34.45	-117.50	P2014	1027	Assumed separate from Harper 3	10	0.97	2	3
South_Mojave	34.30	-117.00	P2014	11237		4	0.04	2	3
Lake Tecopa	35.75	-116.25	P2014	14129		112	0.79	2	3
Lake Mojave	35.05	-116.10	P2014	8219	Assume that Mojave separate from Manly group during Pliocene	120	1.46	2	3
Lake Manix	34.85	-116.40	P2014	1041	Assume that Manix separate from Manly group during Pliocene	50	4.80	2	3
Bristol Lake	34.30	-115.65	P2014	1285		84	6.54	2	3
Cadiz Lake	34.15	-115.40	P2014	967		55	5.69	2	3
Danby Lake	34.05	-115.15	P2014	1120		72	6.43	2	3
Rita Blanca	35.72	-102.39	P2014	1738		54.39	3.13	3	3.6
Hueco Bolson, TX	30.90	-105.30	P2014		Not terminal?	5780		1.8	4.8

Normalized Area (%) Distribution	
Median	4.80
Q1	1.22
Q3	6.48
Max	13.09

**Table DR4 – Climate models used in this study.**

<b>Model</b>	<b>Organization, Country</b>	<b>Atmospheric Resolution (#lat x lon x levels)</b>	<b>References</b>
<b>PMIP3 LGM Ensemble</b>			
CNRM-CM5	CNRM-CERFACS, France	256x128 x L31	Voldoire et al. (2013)
COSMOS-ASO	Freie Universität Berlin, Germany	96x48 x L19	Zhou et al. (2014)
CCSM4	National Center for Atmospheric Research, USA	288x192 x L26	Gent et al. (2011); Brady et al. (2013)
MRI-CGCM3	Meteorological Research Institute, Japan	320x160 x L48	Yukimoto et al. (2012)
IPSL-CM5A-L	Institute Pierre Simon Laplace, France	96x95 x L39	Kageyama et al. (2013); Dufresne et al. (2013)
MPI-ESM-P	Max Planck Institute for Meteorology, Germany	196x98 x L47	
MIROC-ESM	Model for Interdisciplinary Research on Climate, Japan	128x64 x L80	Sueyoshi et al. (2013)
<b>PlioMIP (Experiment 2) Ensemble</b>			
CCSM4	National Center for Atmospheric Research, USA	288x192 x L26	Rosenbloom et al. (2013)
MRI-CGCM 2.3	Meteorological Research Institute and University of Tsukuba, Japan	128x64 x L30	Kamae and Ueda (2012)
NorESM-L	Bjerknes Centre for Climate Research, Norway	96x48 x L26	Zhang and Yan (2012); Zhang et al. (2012)
HadCM3	Hadley Centre for Climate Prediction and Research/Met Office, UK	96x73 x L19	Bragg et al. (2012)
IPSL-CM5A	Institute Pierre Simon Laplace, France	96x95 x L39	Contoux et al. (2012)
COSMOS	Alfred Wegener Institute, Germany	96x48 x L19	Stepanek and Lohmann (2012)

**Table DR5 – Regional fitted Budyko parameters**

<b>Model</b>	<b>LGM <math>\omega</math> value</b>	<b>PI Control <math>\omega</math> value</b>
CNRM-CM5	1.82	2.08
COSMOS-ASO	1.98	2.30
CCSM4	1.98	2.44
MRI-CGCM3	1.97	2.57
IPSL-CM5A-L	1.69	2.21
MPI-ESM-P	1.82	2.31
MIROC-ESM	1.76	2.60
	<b>Pliocene <math>\omega</math> value</b>	<b>PI Control <math>\omega</math> value</b>
CCSM4	2.25	2.60
MRI-CGCM 2.3	2.31	2.27
NorESM-L	1.98	2.18
HadCM3	1.99	1.90
IPSL-CM5A	2.04	2.24
COSMOS	2.64	2.51

## Data Repository References

- Adam, D.P., Bradbury, J.P., Rieck, H.J. and Sarna-Wojcicki, A.M., 1990, Environmental changes in the Tule Lake Basin, Siskiyou and Modoc Counties, California, from 3 to 2 Million years before present, USGS Bulletin 1933, 13 p.
- Allen, B.D., 2005, Ice age lakes in New Mexico: New Mexico's ice ages New Mexico Museum of Natural History and Science Bulletin, no. 28, p. 107-114.
- Braconnot, P., Harrison, S.P., Kageyama, M., Bartlein, P.J., Masson-Delmotte, V., Abe-Ouchi, A., Otto-Bliesner, B., and Zhao, Y., 2012, Evaluation of climate models using palaeoclimatic data: Nature Climate Change, v. 2, no. 6, p. 417-424.
- Brady, E.C., Otto Bliesner, B.L., Kay, J.E., and Rosenbloom, N., 2013, Sensitivity to Glacial Forcing in the CCSM4: Journal of Climate, v. 26, no. 6, p. 1901-1925.
- Bony, S., and Emanuel, K. A., 2001, A parameterization of the cloudiness associated with cumulus convection; evaluation using TOGA COARE data: Journal of the Atmospheric Sciences, v. 51, no. 21, p. 3158-3183
- Bragg, F.J., Lunt, D.J., and Haywood, A.M., 2012, Mid-Pliocene climate modelled using the UK Hadley Centre Model: PlioMIP Experiments 1 and 2: Geoscientific Model Development, v. 5, no. 5, p. 1109-1125.
- Colgan, J.P., Dumitru, T.A., McWilliams, M., Miller, E.L., 2006, Timing of Cenozoic volcanism and Basin and Range extension in northwestern Nevada: New constraints from the northern Pine Forest Range: Bulletin of the Geological Society of America, v. 118, no. 1-2, p. 126-139.
- Contoux, C., Ramstein, G., and Jost, A., 2012, Modelling the mid-Pliocene Warm Period climate with the IPSL coupled model and its atmospheric component LMDZ5A: Geoscientific Model Development, v. 5, no. 3, p. 903-917.
- Dufresne, J.L., Foujols, M.A., Denvil, S., Caubel, A., Marti, O., Aumont, O., Balkanski, Y., Bekki, S., Bellenger, H., Benshila, R., Bony, S., Bopp, L., Braconnot, P., Brockmann, P., et al., 2013, Climate change projections using the IPSL-CM5 Earth System Model: from CMIP3 to CMIP5: Climate dynamics, v. 40, no. 9-10, p. 2123-2165.
- Gent, P., Gent, P.R., Danabasoglu, G., Donner, L.J., Holland, M.M., Hunke, E.C., Jayne, S.R., Lawrence, D.M., Neale, R.B., Rasch, P.J., Vertenstein, M., Worley, P.H., Yang, Z.-L., and Zhang, M., 2011, The community climate system model version 4: Journal of Climate, v. 24, no. 19, p. 4973-4991.
- Gillespie, A., 2014, Land Surface Emissivity, in Njoku, E.G., ed., Encyclopedia of Remote Sensing: Springer Science+Business Media New York, v. XXV, p. 303-311
- Grayson, D., 2011, The Great Basin: a natural prehistory: University of California Press, 432 p.
- Haywood, A., Dowsett, H., and Otto-Bliesner, B., 2011, Pliocene Model Intercomparison Project (PlioMIP): experimental design and boundary conditions (experiment 2): Geoscientific Model Development, v. 4, p. 571-577.
- Haywood, A.M., Hill, D.J., Dolan, A.M., Otto-Bliesner, B.L., Bragg, F., Chan, W.-L., Chandler, M.A., Contoux, C., Dowsett, H.J., Jost, A., Kamae, Y., Lohmann, G., Lunt, D.J., Abe-Ouchi, A., Pickering, S.J., Ramstein, G., Rosenbloom, N.A., Salzmann, U., Sohl, L., Stepanek, C., Ueda, H., Yan, Q., and Zhang, Z., 2013, Large-scale features of Pliocene climate: results from the Pliocene Model Intercomparison Project: Climate of the Past, v. 9, p. 191-209.
- Ibarra, D.E., Egger, A.E., Weaver, K.L., Harris, C.R., and Maher, K., 2014, Rise and fall of late Pleistocene pluvial lakes in response to reduced evaporation and precipitation: Evidence from Lake Surprise, California: Bulletin of the Geological Society of America, v. 126,



- no. 11-12, p. 1387–1415.
- Kageyama, M., Braconnot, P., Bopp, L., Caubel, A., Foujols, M.-A., Guilyardi, E., Khodri, M., Lloyd, J., Lombard, F., Mariotti, V., Marti, O., Roy, T., and Woillez, M.-N., 2013, Mid-Holocene and Last Glacial Maximum climate simulations with the IPSL model—part I: comparing IPSL\_CM5A to IPSL\_CM4: *Climate dynamics*, v. 40, no. 9-10, p. 2447–2468.
- Kamae, Y., and Ueda, H., 2012, Mid-Pliocene global climate simulation with MRI-CGCM2.3: set-up and initial results of PlioMIP Experiments 1 and 2: *Geoscientific Model Development*, v. 5, no. 3, p. 793–808.
- Knott, J.R., Machette, M.N., Klinger, R.E., Sarna-Wojcicki, A.M., Liddicoat, J.C., Tinsley III, J.C., David, B.T., Ebbs, V.M., 2008, Reconstructing late Pliocene to middle Pleistocene Death Valley lakes and river systems as a test of Pupfish (Cyprinodontidae) dispersal hypotheses: *The Geological Society of America Special Paper* v. 439, p. 1-26.
- Koster, R.D., Fekete, B.M., Huffman, G.J., and Stackhouse, P.W., 2006, Revisiting a hydrological analysis framework with International Satellite Land Surface Climatology Project Initiative 2 rainfall, net radiation, and runoff fields: *Journal of Geophysical Research*, v. 111, no. 22, p. D22S05.
- Lehner, B., and Grill, G., 2013, Global river hydrography and network routing: baseline data and new approaches to study the world's large river systems (H. Habersack, D. Walling, & D. Haspel, Eds.): *Hydrological Processes*, v. 27, no. 15, p. 2171–2186.
- Lehner, B., Verdin, K., and Jarvis, A., 2008, New Global Hydrography Derived From Spaceborne Elevation Data: *Eos, Transactions American Geophysical Union*, v. 89, no. 10, p. 93–94.
- Linacre, E.T., 1977, A simple formula for estimating evaporation rates in various climates, using temperature data alone: *Agricultural meteorology*, v. 18, no. 6, p. 409–424.
- Messenger, M.L., Lehner, B., Grill, G., Nedeva, I., and Schmitt, O., 2016, Estimating the volume and age of water stored in global lakes using a geo-statistical approach.: *Nature Communications*, v. 7, p. 13603.
- Mifflin, M.D., and Wheat, M.M., 1979, Mifflin: Pluvial Lakes and Estimated Pluvial Climates of Nevada: *Nevada Bureau of Mines and Geology Bulletin* no. 94, 57 p.
- Milly, P.C.D., and Dunne, K.A., 2016, Potential evapotranspiration and continental drying: *Nature Climate Change*, v. 6, p. 946–949.
- Morcrette, J.-J., 1991, Radiation and cloud radiative properties in the European Centre for Medium Range Weather Forecasts forecasting system: *Journal of Geophysical Research: Atmospheres*, v. 96, no. D5, p. 9121-9132
- Munroe, J.S., and Laabs, B.J.C., 2013, Latest Pleistocene history of pluvial Lake Franklin, northeastern Nevada, USA: *Geological Society of America Bulletin*, v. 125, no. 3-4, p. 322–342.
- Orme, A.R., 2008, Pleistocene pluvial lakes of the American West: a short history of research: *Geological Society, London, Special Publications*, v. 301, no. 1, p. 51–78.
- Phillips, F.M., 2008, Geological and hydrological history of the paleo-Owens River drainage since the late Miocene: *The Geological Society of America Special Paper* v. 439, p. 115-150.
- Reheis, M.C., 1999, Extent of Pleistocene lakes in the western Great Basin: *U.S. Geological Survey Miscellaneous Field Studies Map MF-2323*, scale 1:800,000, 1 sheet.
- Reheis, M.C., Sarna-Wojcicki, A.M., Reynolds, R.L., Repenning, C.A., Mifflin, M.D., 2002,

- Pliocene to middle Pleistocene lakes in the Western Great Basin: Ages and connections, *in* Hershler, R., Madsen, D.B., Currey, D.R., eds., *Great basin aquatic systems history*. Smithsonian Institution Press, Washington D.C., p. 53-108.
- Reheis, M.C., Adams, K.D., Oviatt, C.G., and Bacon, S.N., 2014, Pluvial lakes in the Great Basin of the western United States-a view from the outcrop: *Quaternary Science Reviews*, v. 97, p. 33–57.
- Roderick, M.L., Sun, F., Lim, W.H., and Farquhar, G.D., 2014, A general framework for understanding the response of the water cycle to global warming over land and ocean: *Hydrology and Earth System Sciences*, v. 18, no. 5, p. 1575–1589.
- Roderick, M.L., Greve, P., Farquhar, G.D., 2015, On the assessment of aridity with changes in atmospheric CO<sub>2</sub>: *Water Resources Research*, v. 51, no. 7, p. 5450-5463.
- Rosenbloom, N.A., Otto-Bliesner, B.L., Brady, E.C., and Lawrence, P.J., 2012, Simulating the mid-Pliocene Warm Period with the CCSM4 model: *Geoscientific Model Development Discussions*, v. 5, p. 4269–4303.
- Scheff, J., and Frierson, D. M. W., 2014, Scaling Potential Evapotranspiration with Greenhouse Warming: *Journal of Climate*, v. 27, no. 4, p. 1539-1558
- Smith, G.R., 1981, Late Cenozoic Freshwater Fishes of North America: *Annual Review of Ecology and Systematics*, v. 12, p. 163-193.
- Soller, D.R., Reheis, M.C., Garrity, C.P., and Van Sistine, D.R., 2009, Map database for surficial materials in the conterminous United States: U.S. Geological Survey Data Series 425, scale 1: 5,000,000.
- Stepanek, C., and Lohmann, G., 2012, Modelling mid-Pliocene climate with COSMOS: *Geoscientific Model Development*, v. 5, no. 5, p. 1221–1243.
- Sueyoshi, T., Ohgaito, R., Yamamoto, A., Chikamoto, M.O., Hajima, T., Okajima, H., Yoshimori, M., Abe, M., O'ishi, R., Saito, F., Watanabe, S., Kawamiya, M., and Abe-Ouchi, A., 2013, Set-up of the PMIP3 paleoclimate experiments conducted using an Earth system model, MIROC-ESM: *Geoscientific Model Development*, v. 6, no. 3, p. 819-836.
- Thompson, R.S., 1992, Palynological data from a 989-FT (301-M) core of Pliocene and Early Pleistocene sediments from Bruneau, Idaho, U.S. Geological Survey Open File Report 92-713, 28 p.
- Voldoire, A., Sanchez-Gomez, E., Méliá, D.S.Y., Decharme, B., Cassou, C., Sénési, S., Valcke, S., Beau, I., Alias, A., Chevallier, M., Déqué, M., Deshayes, J., Douville, H., Fernandez, E., et al., 2013, The CNRM-CM5.1 global climate model: description and basic evaluation: *Climate dynamics*, v. 40, no. 9-10, p. 2091–2121.
- Williams, T.R., and Bedinger, M.S., 1984, Selected geologic and hydrologic characteristics of the Basin and Range Province, western United States; Pleistocene lakes and marshes: IMAP 1522-D, scale 1:2,500,000, 1 sheet.
- Yukimoto, S., Adachi, Y., Hosaka, M., Sakami, T., Yoshimura, H., Hirabara, M., Tanaka, T.Y., Shindo, E., Tsujino, H., Deushi, M., Mizuta, R., Yabu, S., Obata, A., Nakano, H., et al., 2012, A New Global Climate Model of the Meteorological Research Institute: MRI-CGCM3–Model Description and Basic Performance: *Journal of the Meteorological Society of Japan*, v. 90A, no. 0, p. 23–64.
- Zhang, Z., and Yan, Q., 2012, Pre-industrial and mid-Pliocene simulations with NorESM-L: AGCM simulations: *Geoscientific Model Development*, v. 5, no. 4, p. 1033–1043.
- Zhang, Z.S., Nisancioglu, K., Bentsen, M., Tjiputra, J., Bethke, I., Yan, Q., Risebrobakken, B.,

- Andersson, C., and Jansen, E., 2012, Pre-industrial and mid-Pliocene simulations with NorESM-L: Geoscientific Model Development, v. 5, no. 2, p. 523–533.
- Zhou, T., Chen, X., Dong, L., Wu, B., Man, W., Zhang, L., Lin, R., Yao, J., Song, F., and Zhao, C., 2014, Chinese contribution to CMIP5: An overview of five Chinese models' performances: Journal of Meteorological Research, v. 28, no. 4, p. 481–509.